Journal of Applied Polymer Science

Significance of polymer on emulsion stability in surfactant-polymer flooding

Yinglong Xuan, Desheng Ma, Minghui Zhou, Ming Gao
State Key Laboratory of Enhanced Oil Recovery, Research Institute of Petroleum Exploration & Development, Beijing, People's Republic of China
Correspondence to: Y. Xuan (E-mail: xuanyinglong100@163.com)

ABSTRACT: The influence of polymer on stability and shear rate on droplet size of emulsion is evaluated in the laboratory, microstructure of the emulsion is observed under a microscope, and the pore distribution of the cores is analyzed through mercury injection experiments. In the process of surfactant-polymer (SP) flooding, the thickness of polymer absorbed on the surface of the rock is calculated by a mathematical model. The experiments show that the polymer is good for the stability of emulsion, with the increase of shear rate, stability becomes better, and droplet size gets smaller. Due to the adsorption of polymer, the pore throat turns narrow, seepage velocity is increasing, and also the emulsion becomes more stable with the smaller-size droplets. During the single emulsifier flooding, the emulsion is easy to coalescence for its instability, and the seepage channel can be easily blocked, which leads to the high injection pressure. Consequently, the polymer plays an important role on emulsion stability in SP flooding. © 2015 Wiley Periodicals, Inc. J. Appl. Polym. Sci. **2015**, *132*, 42171.

KEYWORDS: emulsion polymerization; oil and gas; surfactants; viscosity and viscoelasticity

Received 2 October 2014; accepted 2 March 2015
DOI: 10.1002/app.42171

INTRODUCTION

Many mature reservoirs after water flooding have as much as 50–75% of the original oil still in place. These reservoirs are viable candidates for chemical enhanced oil recovery (EOR) through enlarging sweep volume and improving oil-driving efficiency. However, the design of these chemical mixtures must be tailored to the reservoir rock and fluid (i.e., crude oil and formation brine) properties.[1,2] As one of the most potential technologies, surfactant-polymer (SP) flooding is an important tertiary oil-recovery technique after water flooding and polymer flooding, it is subjected to the value more and more.[3–6] One of the suggested mechanisms is to use oil–water emulsions as a promising drive fluid to improve oil recovery of viscous oils from the reservoirs.[7–11] The polymer solution has better viscoelasticity,[12–14] it can expand the sweep volume[15–17] and surfactant can improve oil displacement efficiencies, as evidenced by its increasing use. From the combination of flooding pilot tests in Daqing oil fields, the recovery had been increased by over 20% after water flooding.[18–21]

McAuliffe[22,23] demonstrated that droplet size has a great influence on recovery by selecting a crude oil–water emulsion as the plug for flooding experiments. The advisable diameters are slightly larger than the size of the porous media. Bragg[24] developed a method to inject an oil–water emulsion into the formation to recover hydrocarbons. The viscosity of the emulsion is lower than the viscosity of crude oil, which reduces the water–oil current ratio. Khambharatana *et al.*[25] discussed the physical mechanisms of the stable emulsion that flows in Berea sandstone and Ottawa sand pack systems and compared the size of the droplets and the porous media. Many researchers[26–29] have explored the flow mechanism of emulsions in a porous medium. The stability of the emulsion is concerned with the shear rate. However, the polymer plays some role in emulsifications of SP flooding. In this work, we mainly devote ourselves to studying the influence of the polymer on the emulsion stability in the process of SP flooding.

The influence of polymer and shear rate on the stability and the droplet size was discussed in bottle tests. To evaluate the performance of emulsion flooding, the throat distribution of the cores was firstly determined by the constant-rate mercury injection experiments and then two sets of flooding experiments with the plug of surfactant-polymer solution and surfactant solution were conducted with the core in a horizontal orientation. The adsorption capacity of polymer in the pore was calculated by the mathematic model. Based on the experiment results and mathematic model, we presented and discussed the significance of polymer on emulsion stability in surfactant-polymer flooding.

EXPERIMENTAL SECTION

Experimental Materials and Equipments

The crude oil used in the experiments was dead oil from the Fuyu oil field (0.86 g/cm^3), with a viscosity of 64.4 mPa·s at 30°C. The brine used in the test was taken from the injection water ($NaHCO_3$ 621.03 mg/L; Na_2SO_4 2.47 mg/L; $MgCl_2{\cdot}6H_2O$ 233.9 mg/L; $CaCl_2$ 215.4 mg/L). An amphoteric ionic emulsifier (chemical structure: R——$(EO)_{18}$) was selected to prepare the emulsions. Polymers of 1200∼1600 × 10^6 molecular weights were used with Berry cores.

Experimental Equipments. RW20 overhead stirrers (IKA, Germany), a C.MAG magnetic rotor mixer (IKA, Germany), a Brookfield DV-II+Proviscometer (Brookfield, United States of America), a DM2500 transmission electron microscope (Leica, Germany), a Zetasizernano (the Malvern, United States of America), an AutoPore IV9500 Mercury Injection Apparatus (Micromeritics, United States of America), and a Quizix pump in the core displacement device were used.

EXPERIMENTAL METHODS

Preparation of Emulsifier and Polymer Solution

The polymer was diluted to 0.3% in injection water solution and agitated by overhead stirrers for 4 hours. The polymer solution was set aside in an incubator at 30°C.

Two types of emulsifier solutions were prepared: a pure emulsifier solution and an emulsifier-polymer solution, in which the polymer concentration was 0.1%. The amphoteric ionic emulsifier was diluted to 0.3% in the injection water solution and agitated under a magnetic rotor mixer for 2 hours before being set aside in an incubator at 30°C.

Determination of Apparent Viscosity

The viscosity of the emulsion at different shear rates was measured in a viscometer (Brookfield DV +) at 30°C.

Determination of Droplet Size

The droplet size at different shear rates was measured by a Zetasizernano at 30°C. The emulsion characteristics were observed under a DM2500 transmission electron microscope.

Determination of Emulsion Stability

Crude oil and emulsifier solutions (a poor emulsifier emulsion and an emulsifier–polymer solution) were mixed at a volumetric proportion of 1:1, stirred at a high speed of 11,000 rpm for 1 minute and set aside in an incubator at 30°C. The volume of water, oil, and emulsion were recorded at different times.

Core Mercury Injection Experiments

The mercury injection curves and the pore throat distributions of two berry cores were measured by an AutoPore IV 9500Mercury Injection Apparatus.

Flooding Experiments

The experimental apparatus (Figure 1) for the core flooding experiments consisted of five sections: a core holder, a displacement pump (Quizix), a pressure pump, cylinders for holding crude oil, water, and emulsifier, and fraction collectors.

The core was first dried in an oven at 100°C for 2 hours. It was then completely saturated with water in self-imbibition process,

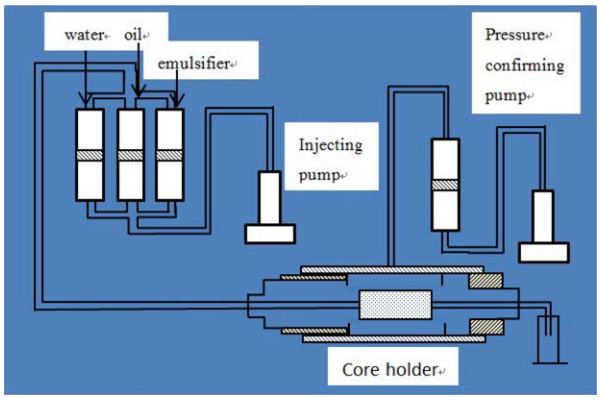

Figure 1. Schematic diagram of crude displacement system. [Color figure can be viewed in the online issue, which is available at wileyonlinelibrary.com.]

and the absolute permeability was measured by injecting water into the water-saturated core at a constant rate of 0.3 mL/min. Afterwards, the core was flooded with crude oil at an injection rate of 0.05 mL/min to saturate it with oil. The core was aged for one day or longer after saturation. Water flooding is conducted with an injection rate of 0.3 mL/min, which was sustained until the water cut was above 98%. After this water displacement, unrecovered residual oil layers were present. The remaining oil was recovered by injecting an emulsifier plug at 0.3 mL/min followed by chase water flooding.

RESULTS

Analyzing the Emulsion Stability

By contrasting the emulsion triggered by the pure surfactant system and the SP binary system, the water drop of an emulsion triggered by pure surfactant was 0.65, while the water drop of an emulsion triggered by the SP binary system was 0.18 (Figure 2), indicating that the inclusion of the polymer is better for the stability of the emulsion.

Crude oil was mixed with the surfactant solution. Under the agitation of external force, oil was dispersed into the water to form the O/W emulsion. The stability of the emulsion is determined by the intensity of the water film, which is influenced by

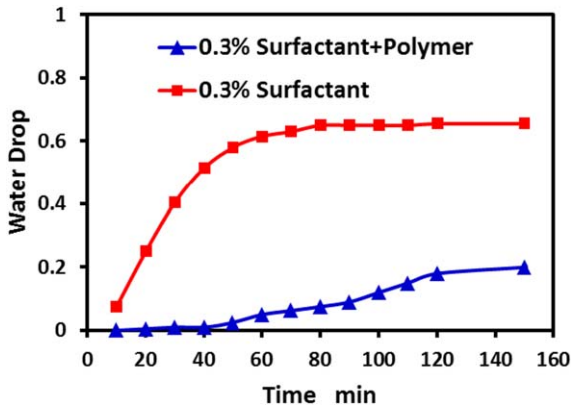

Figure 2. Effect of polymer on water drop of emulsions. [Color figure can be viewed in the online issue, which is available at wileyonlinelibrary.com.]

Table I. Droplet Sizes and Emulsion Types in Different Shear Rates

Shear rate (cm/min)	Shear time (hour)	Droplet size (μm)	Type of emulsion
0.10	2.5	4.6	O/W and W/O
0.15		3.1	O/W and W/O
0.20		1.9	O/W and W/O
0.25		0.89	O/W and W/O

the film strength of the absorbing material and the composition of the water phase. As is reported by Qiu and coworkers,[30–33] the presence of a polymer in the water phase increased the intensity of the water film. As a result, the polymer contributed to the stability of emulsion.

Analyzing the Shear Rate

An emulsifier solution with a concentration of 0.3% was mixed with crude oil at 30°C at a volume ratio of 1 : 1. The analysis of the emulsion at 0.10, 0.15, 0.20, and 0.25 (cm/min) shear rates for 2.5 hours is presented in Table I. As the shear rate increased, W/O and O/W emulsion coexisted (Figure 3) and the viscosity of emulsion dropped gradually. The emulsion viscosity was much lower than that of the crude oil.

The changes in the emulsion droplet size distributions with shearing rate were used as a measure of droplet dispersion in the initial stages. As the emulsions were sheared, part of the oil was emulsified, and W/O and O/W emulsions were both present, the distributions were developed at large droplet sizes, As the shearing rate increased, the stability of the emulsion

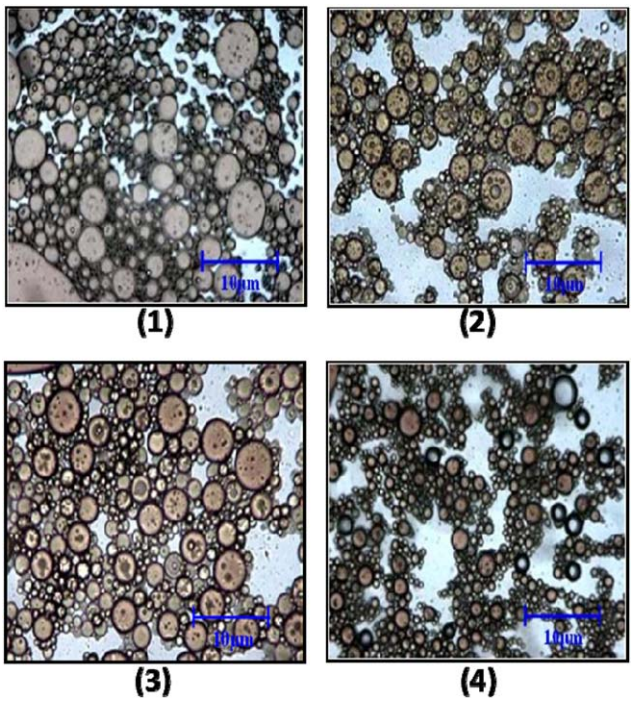

Figure 3. Types of the emulsion at different shear rates. [Color figure can be viewed in the online issue, which is available at wileyonlinelibrary.com.]

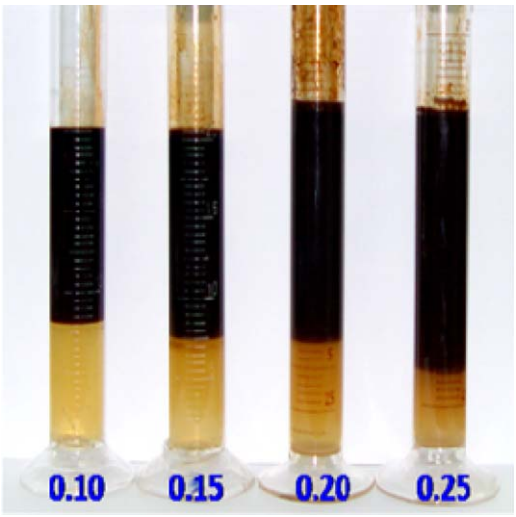

Figure 4. Water drop of emulsions at different shear rates. [Color figure can be viewed in the online issue, which is available at wileyonlinelibrary.com.]

increased (Figures 4 and 5) and the population of larger drops shifted to smaller sizes (Figures 6). As the shear rate continued to increase, droplets became smaller and the superficial area grew larger. When the emulsifier was not sufficient to keep the coalescence of oil drops, the O/W slowly reverted to W/O (i.e., a phase reversal). The effect of shear rate on droplet size and water drop was simultaneously shown in Figure 7.

With the increasing of the stirring intensity, the droplet size of the oil becomes smaller and the emulsion turns more stable. However, if the stirring intensity is too great and the energy input is too much, it causes the energy-wasting and negative economic problems. In addition, the emulsion is too stable to present difficulties for dehydration operations. At a certain stirring intensity, the longer the stirring time, the more stable the emulsion.

Analyzing the Mercury Injection Experiments

A statistical analysis of the mercury injection data reveals the physical properties and pore structures of the cores. Because the core permeability is low, the average pore radius is narrow and

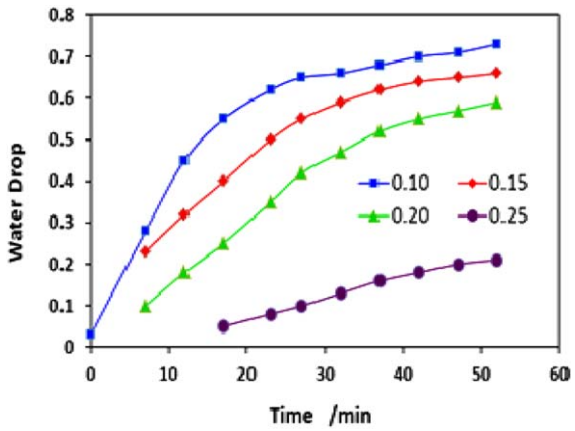

Figure 5. Changes of water drop at different shear rates. [Color figure can be viewed in the online issue, which is available at wileyonlinelibrary.com.]

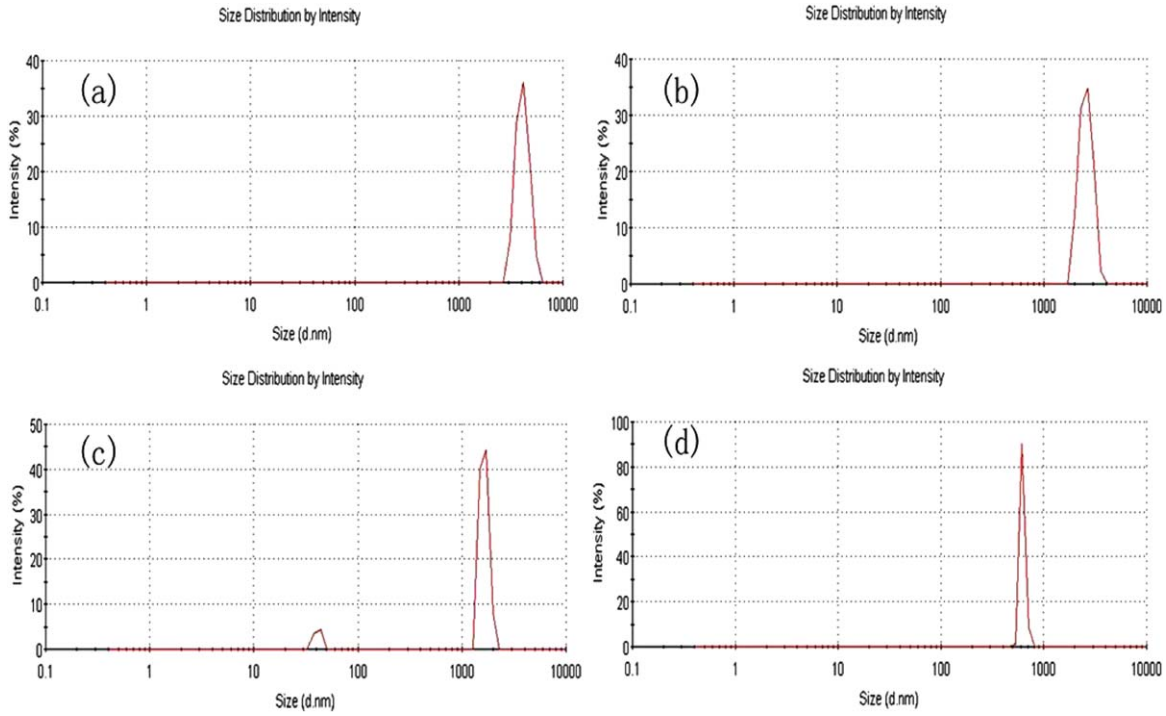

Figure 6. Droplet size distribution at different shear rates of (a) 0.10 (cm/min); (b) 0.15 (cm/min); (c) 0.20 (cm/min); and (d) 0.25 (cm/min). [Color figure can be viewed in the online issue, which is available at wileyonlinelibrary.com.]

prevents the visualization of a few parameter scans. However, the mercury injection curves and the distribution of the pore radius are clearly identifiable. For core 1, the pore radius median is 7.33 (μm) [Figure 8(a)], the displacement pressure is 0.063 (MPa), and the median saturation pressure is 0.1 (MPa). For core 2, the pore radius median is 6.696 (μm) [Figure 8(b)], the displacement pressure is 0.062 (MPa), and the median saturation pressure is 0.11 (MPa).

Analyzing the Flooding Experiments

To evaluate the performance of emulsion flooding, two sets of flooding experiments were conducted with the core in a horizontal orientation. These experiments investigated the continuous displacement of crude oil by water flooding, chemical flooding, and subsequent water flooding.

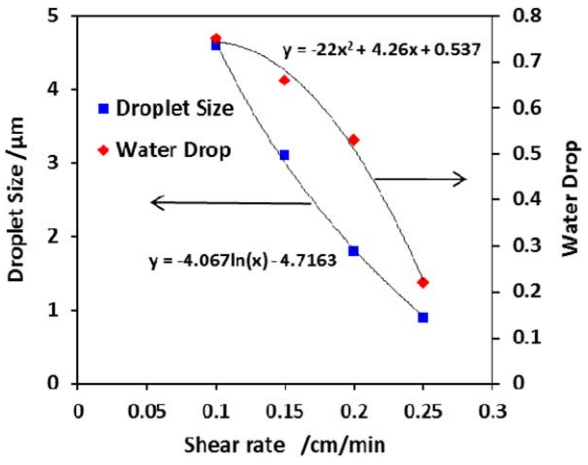

Figure 7. Effect of shear rate on droplet size and water drop. [Color figure can be viewed in the online issue, which is available at wileyonlinelibrary.com.]

In the first experiment, the plug was a solution with a surfactant concentration of 0.3% and 1000 ppm polymer. The plug valued 50% of the pore volume, the injecting rate was controlled at 0.3 (mL/min), the experiments were conducted in an oven at 30°C. In the second experiment, the plug was a solution with a surfactant concentration of 0.3% without polymer, and the other injection parameters were the same as in the first experiment.

Prior to oil saturation, routine measurements for determining the rock permeability to water were conducted for each core. The physical parameters of each core, containing porosity φ, permeability K, and other parameters were given in Table II. All experiments were conducted in cores with approximately 19% porosity and $148\sim164\times10^{-3}$ (μm^2) permeability. The water flooding recovered nearly 50% of the original oil in place. After water-cut exceeded 98% in water flooding, the rock was subsequently flooded with emulsifier or SP combination plugs followed by chase water. The recovery of the oil and water fractions with pore volume injections for the two different systems was presented in Figures 9 and 10. After water breakthrough, the water fraction sharply increased above 90% in each case. The water viscosity was much lower than that of the crude oil (64.4 mPa·s) at the test temperature. As a result, the long transient production during water flooding may be due to the unfavorable mobility ratio between the injected water and crude oil. The obvious water precipitation reduction and oil increase were achieved in plug displacement.

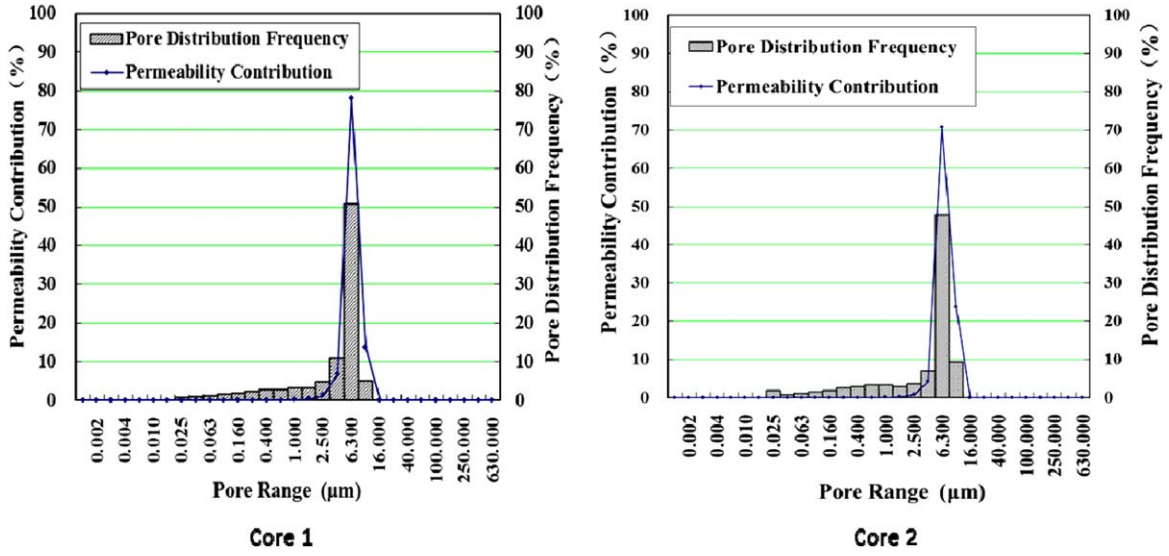

Figure 8. Distribution of the pore radius. [Color figure can be viewed in the online issue, which is available at wileyonlinelibrary.com.]

As shown in Figures 9 and 10, the water flooding recovery and the ultimate recovery were 50.9% and 76.3% in SP flooding experiment, and the water flooding recovery and the ultimate recovery were 49.8% and 74.6% in emulsifier flooding experiment. The detailed results of the different systems are given in Table II. The pressure curves were shown in Figures 9(b) and 10(b), they had the significant differences. In the SP flooding experiment, the viscosity of the plug was 17.9 mPa·s which was more viscous than that of water, the injection pressure rose with the increase of the plug volume and then researched a certain value. The injection pressure dropped in the process of chase water flooding. In emulsifier flooding experiment, the viscosity of the plug was 1.5 mPa·s, which was approximately of the same value as water, the injection pressure had a brief rising as the increase of the plug volume, and then the pressure dropped. When the injection volume researched 0.7 PV (pore volume), the pressure began to rise again, and the injection pressure continued to rise rapidly in the process of chase water flooding. This illustrated that the formed emulsion blocked the core in emulsifier flooding.

Analyzing the Polymer Adsorption Model

Polymer flooding is dependent on the degree of adsorption in the reservoir. Based on fluid transfusion power law in a circular tube, the flow formula and the dynamic adsorption properties of the polymer is derived in porous media using the properties of capillary action and the properties of the polymer material.

The reservoir rock is assumed to be composed of a group of smooth, parallel capillary tubes of the same length as the rock, but with different radius. For a capillary tube with a radius of R_i meters, the polymer follows the characteristics of a power law fluid as it flows through the capillary tubes:[34–36]

$$q_i=\pi\left(\frac{\Delta P}{2KL\lambda}\right)^{\frac{1}{n}}\frac{n}{1+3n}\frac{V_i}{L}\left(\frac{2\sigma\ \cos\theta}{P_{cbi}}\right)^{\frac{1+n}{n}} \quad (1)$$

The polymer is a type of macromolecule. When it flows in the porous media, only polymer molecules with radius (R_p) smaller than the capillary tubes can seep through the rock. Before the polymer is injected, the capillary pressure of the tubes of radius R_p is $P_{cp}=2\sigma\cos\theta/R_p$. Based on the curve of P_c vs. S_w, the value of P_{cp} can be calculated by the saturation S_{wbp} and S_{wap} (Figure

Table II. Flooding Results of the Different Systems

Core	Porosity (%)	Permeability k_w (10^{-3} μm^2)	Plug		Viscosity/ mPa·s	Recovery of oil after water flooding at 98% water cut (% OOIP)	Highest displacement pressure (MPa)	Ultimate recovery (% OOIP)
1	18.87	148	0.5 PV	0.3% Emulsifier+ 0.1% Polymer	17.9	50.9	1.39	76.3
2	20.13	164	0.9 PV	0.3% Emulsifier	1.5	49.8	2.2	74.6

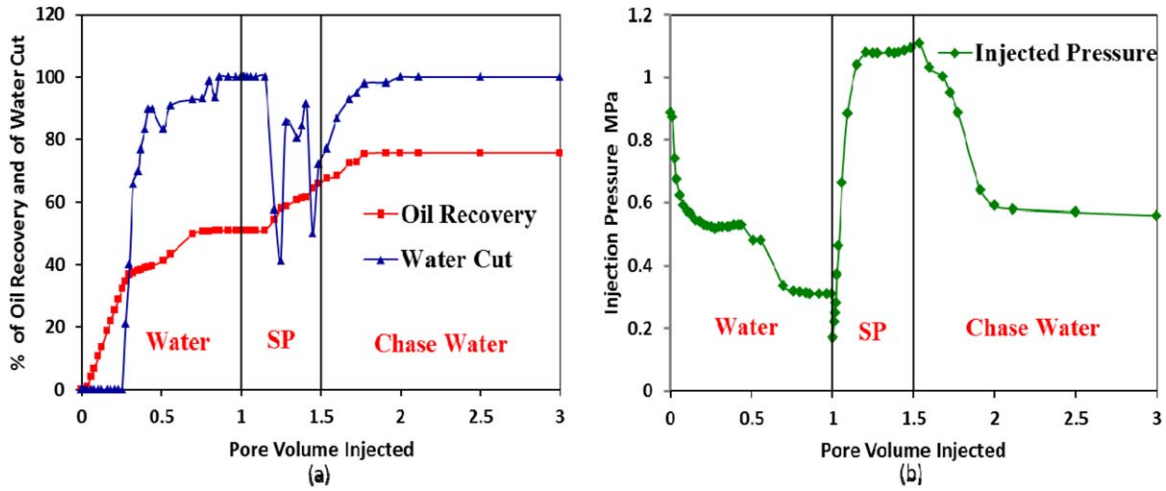

Figure 9. Production performance of SP combination flooding. [Color figure can be viewed in the online issue, which is available at wileyonlinelibrary.com.]

11). Assuming that $B=\left(\frac{1}{P_{cbi}}\right)^{\frac{1+n}{n}}$ and $A=\left(\frac{1}{P_{cai}}\right)^{\frac{1+n}{n}}$, when the size and dynamic adsorption of the polymer is considered, the flux of the polymer that seeps through the rock under pressure ΔP is then:

$$V_m=\Delta T\left(\frac{\Delta P}{2KL\lambda}\right)^{\frac{1}{n}}\frac{nA\phi}{1+3n}(2\sigma\cos\theta)^{\frac{1+n}{n}}\int_{S_{wbp}}^{1}BdS_w \quad (2)$$

$$V_{mo}=\Delta T\left(\frac{\Delta P}{2KL\lambda}\right)^{\frac{1}{n}}\frac{nA\phi}{1+3n}(2\sigma\cos\theta)^{\frac{1+n}{n}}\int_{S_{wap}}^{1}AdS_w \quad (3)$$

The formula that is used to determine the dynamic adsorption in the porous medium is

$$A_p=\frac{V_m-V_{mo}}{V}=\frac{\int_{S_{wbp}}^{1}BdS_w-\int_{S_{wap}}^{1}AdS_w}{\int_0^1 BdS_w} \quad (4)$$

where q_i is the flux of the polymer that seeps through the capillary tubes with a radius of R_i (m^3/s), ΔP is the pressure drop of the polymer seeping through the rocks (Pa), K is the consistency coefficient of the polymer (Pa·s), n is the flow index, L is the length of the rock (m), V_i is the pore volume (m^3), σ is the oil-water interfacial tension (N/m), θ is the contact angle (°), P_{cbi} is the capillary pressure before polymer is injected (Pa), φ is the porosity of the rock, V_m is the volume of the polymer that flows through the rocks regardless of adsorption (m^3), V_{mo} is the volume of the polymer that flows through the rocks with adsorption (m^3), and A_p is the dynamic adsorption of the polymer per unit volume of porous medium (cm^3/cm^3).

Assuming that the core is composed of a group of capillary tubes, the average pore radius, respectively, is 7.330 (μm) and 6.696 (μm) according to the mercury injection curve. For core 1, the diameter is 3.81 (cm), the length is 20.25 (cm), the

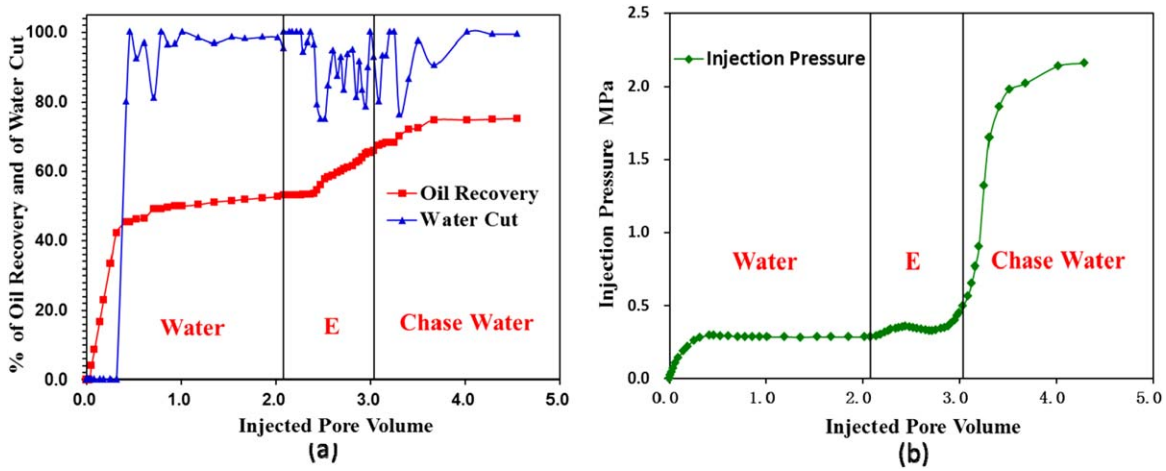

Figure 10. Production performance of emulsifier flooding. [Color figure can be viewed in the online issue, which is available at wileyonlinelibrary.com.]

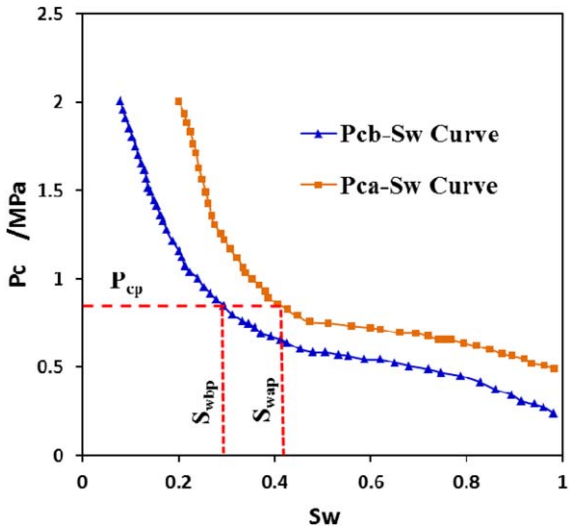

Figure 11. Capillary pressure curve. [Color figure can be viewed in the online issue, which is available at wileyonlinelibrary.com.]

porosity is 18.87%, and the volume of the core is 43.54 (cm^3), which is calculated by formula (5):

$$V_\phi = \frac{1}{4}\phi\pi d^2 L \tag{5}$$

where d is the diameter of the core (cm) and L is the length of the core (cm).

According to Table III, the dynamic adsorption of the polymer is 278.37 ($\mu g/cm^3$) in core 1, and the total volume of adsorbed polymer is 12.12 (cm^3), which is calculated by formula (6).

$$V_{\text{absorption}} = \frac{V_\phi \times \nu_{\text{dynamic adsorption}}}{C_{\text{polymer concentration}}} \tag{6}$$

The volume and the radius of the core is decreased due to the adsorption of the polymer, and the theoretical value of the pore volume is 31.42 (cm^3), which is calculated by the formula $V_{\text{theory}} = V_\phi - V_{\text{absorption}}$. The equivalent porosity is 13.62%, and the equivalent radius is 5.290 (μm), which is based on formula (7).

$$R_{\text{equivalent radius}} = \frac{R(V_\phi - V_{\text{absorption}})}{V_\phi} \tag{7}$$

One-dimensional shear velocity is calculated by formula (8), and the results are shown in Table IV.

$$S = \frac{4V_{\text{injection}}}{\phi\pi d^2} \tag{8}$$

In the process of SP flooding, oil–water emulsification appeared under the shear force. As shown in Figure 2, the emulsion stability nearly tripled, compared with the emulsion without polymer. As a result, the emulsion was relatively stable. The pore volume and flow channel of the core is narrowed due to the adsorption and retention of the injected polymer. This is equivalent to increase the shear rate in the core at the same flooding rate. During the course of the experiments, the plug was injected at a rate of 0.3 (mL/min), which is equivalent to the shear rate of 0.14 (cm/min). The adsorbing capacity of the polymer was calculated by formula (7), the pore radius was narrowed form 7.33 (μm) unadsorbed to 5.29 (μm) adsorbed. Calculated by formula (8), the shear rate in the flow channel was raised from 0.14 (cm/min) to 0.19 (cm/min). As shown in Figure 7, droplet size of the emulsion was decreased from 3.826 (μm) to 2.056 (μm). The reduction of droplet size had increased the stability of the emulsion for 1.5 times. As a result, the emulsion stability had been increased by 4.5 times and the injected pressure was stable in core 1, and the obvious blocking phenomenon did not happen.

The plug without polymer was injected into core 2 at a shear rate of 0.14 (cm/min), and oil–water emulsification appeared under the shear force. The shear rate was smaller than core 1 and there was no stabilizer such as polymer, which resulted in larger droplet sizes and poorer emulsion stability. Therefore, droplets of the emulsion could easily coalesce into large droplets and block the pore throat, which caused the injection pressure to increase.

As shown in Figure 7, with the increase of injecting rate, the droplet size and viscosity of the emulsion become smaller, and the stability of the emulsion gets better. So, for single emulsifier flooding, it can be considered to improve the injection rate to overcome the blocking problem caused by the demulsification and the coalescence.

DISCUSSION

Based on the presented results, a mechanism of polymer adsorption on the stability of emulsion is proposed and shown in Figure 12. There is a large amount of residual oil remaining in the formation after long-term water flooding. Chemical flooding is used to enhance oil recovery. An SP system is injected into the formation [Figure 12 (a)]. The polymer is adsorbed and retained on the pore surface, which reduces the pore radius [Figure 12 (c)]. Meanwhile, the polymer acts as a sacrificial agent to reduce the adsorption of the surfactant. The reduction of the pore radius corresponds with the increase in seepage velocity and emulsification is enhanced [Figure 12 (b)]. Droplet size is relatively small and the presence of the polymer

Table III. Calculation of Polymer Dynamic Adsorption

			Polymer			
Core	Permeability (10^{-3} μm^3)	Porosity (%)	Type	Molecular weight	Concentration ($\mu g/cm^3$)	Dynamic adsorption capacity ($\mu g/cm^3$)
1	148	18.87	3330S	12×10^6	1000	278.37

Table IV. Calculation of Shear Rate in the Cores

Core	Injection rate (mL/min)	Diameter (cm)	Equivalent porosity	Shear rate (cm/min)	Stability (%)
1	0.3	3.81	13.62%	0.19	0.42
2	0.3	3.65	20.13%	0.14	0.69

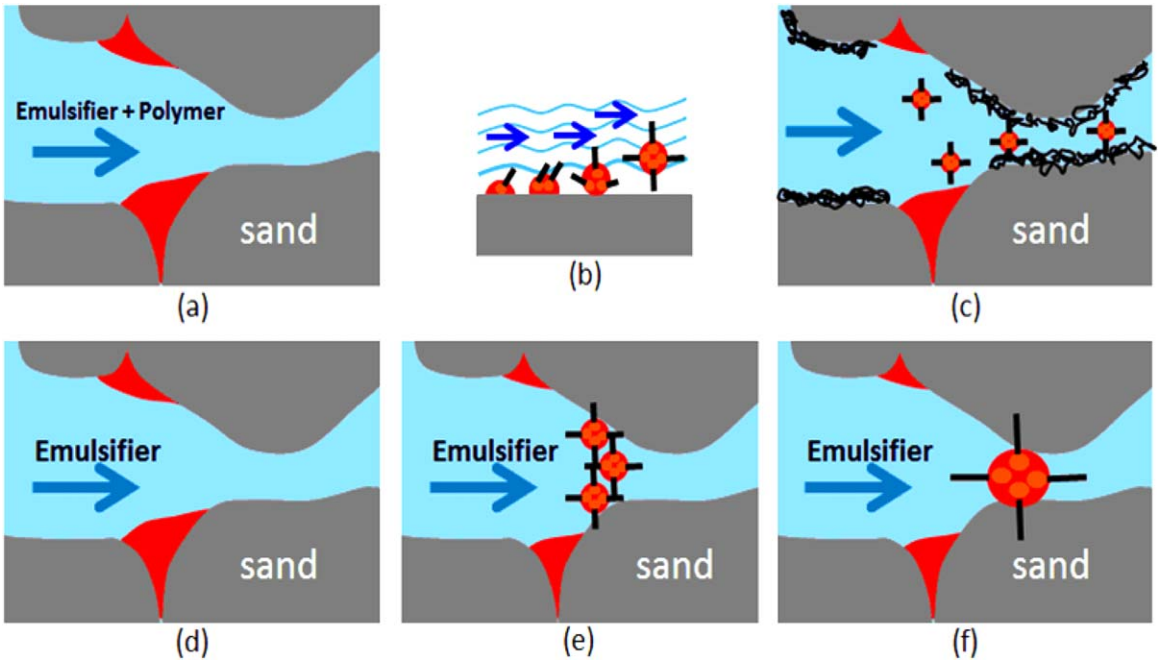

Figure 12. Mechanism of polymer adsorption on the stability of emulsion. [Color figure can be viewed in the online issue, which is available at wileyonlinelibrary.com.]

increases the stability of emulsion. Therefore, the emulsion has a stable seepage in the pore. SP flooding has the effect of moving the residual oil and enhancing oil recovery. When the single emulsifier solution is injected into the formation [Figure 12 (d)], part of the residual oil is emulsified, but the emulsion is not stable because the shear rate is relatively slow and there is no sacrificial agent or stabilizer present, such as a polymer. The emulsion readily coalesces into large droplets [Figure 12 (e)] that block the seepage channel [Figure 12 (f)]. As a result, the injection pressure increases.

CONCLUSIONS

Based on this investigation, the following conclusions can be drawn.

1. The presence of the polymer in the water phase increases the intensity of the water film and the viscosity of the emulsion. The stability of the emulsion is increased.
2. As the shear rate increases, the mechanical shear on the oil increases, leading to smaller droplet sizes and an increased emulsion stability.
3. Polymer adsorption in the pore reduces the pore volume, which has the same effect as that observed when increasing the shear rate. The polymer acts as a sacrificial agent and stabilizer, increasing the stability of the emulsion during SP flooding.
4. For single emulsifier flooding, the emulsion is not stable and readily coalesces into large droplets, which will block the seepage channel. The single emulsifier flooding can enhance the injection pressure and expand the sweep volume. It can be considered to improve the injection rate to overcome the blocking problem caused by the demulsification and the coalescence.

REFERENCES

1. Flaaten, A.; Nguyen, Q. P.; Pope, G. A.; Zhang, J. *SPE Reservoir Eval. Eng.* **2009**, *12*, 713.
2. Watkins, C. *Inform* **2009**, *11*, 682.
3. WU, W.; MA, K. Power and Energy Engineering Conference. 2010, APPEEC5449151, 1.
4. Yin, D.; Peng, B.; Qin, H. International Conference on Advanced Computer Theory and Engineering. 2010, ICACTE 5579859, 510.
5. Wang, Y.; Zhao, F.; Bai, B. SPE 127391 presented at SPE Improved Oil Recovery Symposium, Tulsa, Oklahoma, USA, April 24–28, **2010**.

6. Feng, A.; Zhang, G.; Ge, I.; Ping, J.; Pei, H.; Zhang, J.; Li, R. In SPE 157621 presented at SPE Heavy Oil Conference Canada, Calgary, Alberta, Canada, June 12–14, **2012**.
7. Austad, T.; Strand, S. *J. Colloids Surf. A* **1996**, *108*, 243.
8. Santanna, V. C.; Curbelo, F. D. S.; Castro Dantas, T. N.; Dantas Neto, A. A.; Albuquerque, H. S.; Garnica, A. I. C. *J. Petrol. Sci. Eng.* **2009**, *66*, 117.
9. Daripa, P. Proceedings of 6th IMACS International Symposium on Computer Methods for Part. Diff. Eq.-VI; Vichnevetsky, R., Ed.; Bethlehem, PA, **1987**; p 411.
10. Daripa, P.; Glimm, J.; Lindquist, B.; McBryan, O. *SIAM J. Appl. Math.* **1988**, *48*, 353.
11. Daripa, P.; Glimm, J.; Lindquist, B.; Maesumi, M.; McBryan, O. The IMA Volumes in Mathematics and Its Applications, Vol. *11*; Springer: New York, **1988**; p 89.
12. Qiu, L.; Shao, Z.; Wang, J.; Zhang, D.; Cao, J. *Acta Chim. Sinica.* **2013**, *71*, 1521.
13. Qiu, L.; Shao, Z.; Wang, P.; Wang, D.; Zhou, Z.; Wang, F.; Wang, W.; Wang, J. *Carbohydr. Polym.* **2014**, *110*, 121.
14. Qiu, L.; Shao, Z.; Wang, D.; Zhou, Z.; Wang, F.; Wang, W.; Wang, J. *Carbohydr. Polym.* **2014**, *112*, 532.
15. Zhao, G.; Dai, C.; Zhao, M. *PLoS One.* **2014**, *9*, e100471.
16. Zhao, G.; Dai, C.; Zhao, M.; You, Q. *Molecules.* **2012**, *17*, 14484.
17. Dai, C.; Zhao, G. *J. Appl. Polym. Sci.* **2013**, DOI: 10.1002/app.40154.
18. Cheng, J.; Li, Q.; Liao, G.; Yang, Z.; Yao, Y.; Xu, D. *Petrol. Geol. Oilfield Dev. Daqing.* **2001**, *20*, 46.
19. Cheng, J.; Wang, D.; Li, Q. *Acta Petrol. Sin.* **2002**, *23*, 37.
20. Li, S.; Yang, Z.; Song, K.; Kang, W. *Acta Petrol. Sin.* **2003**, *24*, 71.
21. Wang, K.; Fu, T.; Wang, C.; Ming, Y. *Oilfield Chem.* **2013**, *31*, 83.
22. McAuliffe, C. D. *J. Petrol. Technol.* **1973**, *25*, 721.
23. McAuliffe, C. D. *Petrol. Sci. Technol.* **1973**, *25*, 727.
24. Bragg, J. R. US Patent 5927404. **1998**.
25. Khambharatana, F.; Thomas, S.; Nad Farouq Ali, S. M. SPE 48910 presented at SPE International Oil and Gas Conference and Exhibition in China, Beijing, November 2–6, **1998**.
26. Devereux, O. F. *Chem. Eng. J.* **1974**, *7*, 129.
27. Soo, H.; Radke, C. *J. Ind. Eng. Chem. Fund.* **1974**, *23*, 342.
28. Krieger, I. M.; Dougherty, T. *J. Trans. Soc. Rheol.* **1859**, *3*, 137.
29. Pal, R. *Chem. Eng. J.* **2001**, *81*, 15.
30. Qiu, J. *Petrol Sci Technol.* **2013**, *31*, 142.
31. Chatterji, J.; Borchardt, J. K. *J. Petrol. Technol.* **1981**, *33*, 2042.
32. Djuve, J.; Yang, X.; Fjillanger, I. *Colloid Polym. Sci.* **2001**, *279*, 232.
33. Xia, L.; Lu, S.; Cao, G. *J. Colloid Interface Sci.* **2004**, *271*, 504.
34. Lopez, X.; Valvatne, P. H.; Blunt, M. J. *J. Colloid Interface Sci.* **2003**, *264*, 256.
35. Hirasaki, G. H.; Pope, G. A. *SPE J* **1974**, *14*, 337.
36. Wang, Y. *Drill. Prod. Technol.* **1997**, *20*, 30.